Journal of Innovative Optical Health Sciences
Vol. 13, No. 2 (2020) 2050004 (11 pages)

DOI: 10.1142/S1793545820500042

Improving sampling depth of laser speckle imaging by topical optical clearing: A theoretical and *in vivo* study

D. Li, Y. Zhang and B. Chen*
State Key Laboratory of Multiphase Flow in Power Engineering
Xi'an Jiaotong University
Xi'an, Shaanxi 710049, P. R. China
**chenbin@mail.xjtu.edu.cn*

Received 29 August 2019
Accepted 10 November 2019
Published 26 December 2019

The effect of optical cleaning method combined with laser speckle imaging (LSI) was discussed to improve the detection depth of LSI due to high scattering characteristics of skin, which limit its clinical application. A double-layer skin tissue model embedded with a single blood vessel was established, and the Monte Carlo method was used to simulate photon propagation under the action of light-permeating agent. 808 nm semiconductor and 632.8 nm He–Ne lasers were selected to study the effect of optical clearing agents (OCAs) on photon deposition in tissues. Results show that the photon energy deposition density in the epidermis increases with the amount of tissue fluid replaced by OCA. Compared with glucose solution, polyethylene glycol 400 (PEG 400) and glycerol can considerably increase the average penetration depth of photons in the skin tissue, thereby raising the sampling depth of the LSI. After the action of glycerol, PEG 400, and glucose, the average photon penetration depth is increased by 51.78%, 51.06%, and 21.51% for 808nm, 68.93%, 67.94%, and 26.67% for 632.8 nm lasers, respectively. *In vivo* experiment by dorsal skin chamber proves that glycerol can cause a substantial decrease in blood flow rate, whereas PEG 400 can significantly improve the capability of light penetration without affecting blood velocity, which exhibits considerable potential in the monitoring of blood flow in skin tissues.

Keywords: Laser speckle image; topical optical clearing; imaging depth; Monte-Carlo simulation; dorsal skin experiment.

1. Introduction

Port-wine stain (PWS) is a congenital skin vascular malformation with occurrence rate of 0.3%–0.5% in neonates.[1,2] PWSs are mainly found in the face and neck which seriously affects the normal life of patients. Effective treatment can be achieved by laser therapy in which the disordered blood vessels can be blanched due to the laser energy absorption

*Corresponding author.

by hemoglobin without causing damage to the surrounding normal tissues.[3] Optimization of laser parameters depends on the vessel morphology and online monitoring of blood flow.[4] However, current empirical treatment leads to low cure rate of PWS (still less than 20%) due to the lack of effective imaging techniques.[5]

Briers proposed noninvasive laser speckle imaging (LSI),[6] which has considerable potential in monitoring blood flow and vascular diameter change in skin tissues. When laser irradiates a blood vessel, red blood cell motion (coherent superposition of light scatterers) will lead to light intensity fluctuation of the speckle pattern. Through statistical analysis of image contrast, high spatial and temporal resolutions can be achieved without contrast agent, scanning, or contacting.[7–10]

At present, LSI technology has been widely used in blood flow monitoring of skin,[9] cortex,[11] and mesentery.[12] Blood flow imaging in tissue offers valuable functional information for diagnosing and assessing many diseases including cardiology, small bowel resection (SBR), etc. However, the penetration depth in the skin is limited due to the high scattering characteristics of skin tissues. The detection depth of LSI can only reach 300 μm,[13] which is insufficient to cover the buried depth range (100–1000 μm) of PWS vessels.

Several methods are currently used to increase the sampling depth of LSI. Changing the LSI system from reflection to transmission mode can effectively increase the sampling depth, but implementing this change for *in vivo* detection is difficult. Linear light source scanning combined with lateral indirect illumination can remove the reflected light from the surface, thereby improving the penetration depth. However, this method requires an additional scanning device.

Increasing the depth of LSI is difficult due to the high scattering characteristics caused by the mismatched refractive index of background (such as cytoplasm and interstitial cells) and scattering (such as collagen and elastic fibers) components of skin tissues. Introduction of high-permeability and high-refractive-index optical clearing agents (OCAs) can improve the matching degree of the refractive index, thereby reducing scattering and increasing light penetration depth in skin tissues. After early studies by Tuchin *et al.*[15] much effort has been devoted to the investigation of optical cleaning effects. Vargas *et al.*[16] injected glycerol into hamster skin and found that the transmission coefficient of skin increases by 50%. Galanzha *et al.*[17] applied glucose solution with different concentrations (20%, 25%, 30%, 35%, and 40%), and 75% of glycerol went to the mesenteric vessel of rats. The blood flow velocity may be observed for a stagnation period. Feng *et al.*[18] used disaccharides as OCA and demonstrated that sucrose could cause a more significant increase in imaging depth and signal intensity than fructose. Cheng *et al.*[19] studied the effect of glycerin on cerebral blood flow after different times of dura mater in rabbits by LSI. They found that the velocity of cerebral blood flow decreases with the increase in glycerol amount. Wang *et al.*[20] gives an overview of recent progress in the use of tissue optical clearing (TOC) for vascular visualization with LSI. Shi *et al.*[21] demonstrate the capability of a combination method of LSI and skin optical clearing to describe in detail the dynamic response of cutaneous vasculature to vasoactive noradrenaline injection. Yu *et al.*[22] demonstrated that simultaneous application of OCAs and wavefront shaping techniques in optical coherence tomography (OCT) can provide significant enhancement of penetration depth and imaging quality. Guo *et al.*[23] used a mixture of fructose with PEG-400 and thiazone (FPT) as an optical clearing agent in mouse dorsal skin and the observation showed that the mixture OCA leads to an improved imaging performance in OCT angiography for the deeper tissues. The propagation and deposition of photons in the skin cannot be observed from the experiments. Studying the effect of OCAs on blood vessels with different depths and diameters using experimental methods is time consuming and difficult. By comparison, numerical simulation can be conducted to investigate the photon transmission directly after the action of OCA on the skin tissue which quantitatively evaluates the cleanup degree. In combination with experimental observation, suitable OCA can be efficiently decided.

A double-layer skin tissue model with a single blood vessel was established in this study. Glycerol, PEG 400 (polyethylene glycol), and 40% glucose, which are safe for the human body[24] and have been used in medicine and cosmetics, were taken as examples. The photon transport and deposition of blood vessels with different diameters and buried depths were simulated by Monte Carlo method to check the effect of OCA on LSI which will provide

theoretical guidance to increase the sampling depth of LSI.

2. Numerical Simulation of Photon Transmission in Skin Tissues

2.1. *Skin model*

The numerical analysis of a typical laser PWS surgery process was based on a two-layered skin model shown in Fig. 1. The skin model consists of two layers: an epidermal layer containing melanin and a dermal layer containing a single PWS blood vessel. PWS blood vessel was idealized to be a cylinder. The thicknesses of epidermis and dermis are 60 and 1440 μm, respectively. One single vessel with a diameter of 100 μm was buried in the dermis at the laser spot center parallel to the skin surface in the depth of 1 mm. The computational domain is $1.4 \times 1.4 \times 1.5$ mm and the laser spot diameter is 1 mm.

Choosing a light source with high scattering characteristic of erythrocytes, which is the main scattering factor in blood vessel imaging, is important for LSI. In this work, 808 nm semiconductor and 632.8 nm He–Ne lasers were selected to study the effect of OCAs on the photon deposition in tissues. Erythrocytes are the main scatterers in the application of blood flow imaging. The high absorption in 632.8 nm wavelength by erythrocytes could guarantee accurate measurements of blood flow velocity. The 808 nm semiconductor laser has weaker absorption but larger penetration than that of the 632.8 nm He–Ne laser, which is beneficial for imaging of the deep-buried vessel in practice. For erythrocytes, 632.8 nm light has high absorption coefficients, which could guarantee accurate measurements of blood flow velocity. The 808 nm semiconductor laser has lower absorption coefficients but larger penetration than those of the 632.8 nm He–Ne laser, which is beneficial for imaging the deep-buried vessel in practice.

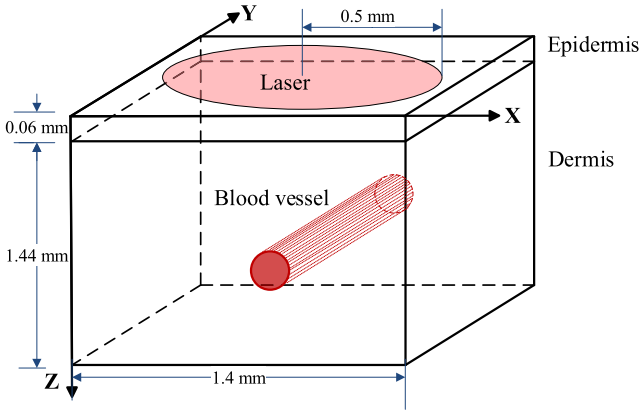

Fig. 1. Two-layer skin model with single discrete vessel.

The optical properties of different chromophores in skin tissues affect laser absorption by the skin. In this work, the content of melanin in the epidermis is 5%, and the specific volume of erythrocytes in blood vessels is 45%. The optical properties of each layer of skin tissue under laser wavelengths of 808 and 632.8 nm are shown in Table 1, where μ_a, μ_s, and g are the absorption coefficient, scattering coefficient, and anisotropic factor, respectively, and n is the refractive index.

2.2. *Monte Carlo simulation*

The Monte Carlo method[26] was used in this study to simulate photon transmission in skin tissues. At the beginning of the simulation, all photons are given a weight value. Photon energy will be reduced because of collision, tissue absorption, and scattering, while the transmission direction is changed due to reflection and transmission. When photons reach the epidermis–dermis or dermis–vessel boundary, photon penetration in the boundary or reflection by the incident direction and step size of photons at the interface are determined. The average depth of photon propagation in the tissue can be obtained by averaging the depth reached in each photon scattering event. The maximum depth is the highest probability of occurrence in the average depth of all photons.[27]

2.3. *Optical property change by adding OCA*

As previously mentioned, the skin is a highly scattered medium. The limited light transmission in

Table 1. Optical properties of skin tissues irradiated by 808/632.8 nm lasers.[25]

	Epidermis	Dermis	Blood
$\mu_a(\text{mm}^{-1})$	0.7104/1.579	0.0248/0.031	0.454/2.175
$\mu_s(\text{mm}^{-1})$	9.198/12.742	9.198/12.742	61.598/85.657
g	0.85/0.80	0.85/0.80	0.98/0.99
n	1.37/1.37	1.37/1.37	1.33/1.33

skin tissues is due to the mismatch in refractive index between collagen fibers, organelles, nuclei and cytoplasm, and tissue fluids.[26] When OCA acts on the tissue, water in the tissue will flow from the cell gap to the tissue surface or overflow. This phenomenon increases osmotic pressure and decreases the water content in the intercellular space and the refractive index difference. Thus, the scattering of photons in skin tissues is reduced, and the penetration depth is increased. In the numerical simulation, the effect of OCA on photonic transmission in the tissue is studied by replacing the moisture in the tissue with OCAs, such as glycerol PEG 400 and glucose solution. According to the improved Gladstone and Dale theorem,[28] the refractive index n of each layer of the organization is as follows:

$$n_k = (1 - W_k)n_{Tk} + XW_k n_a + (1 - X)W_k n_w, \quad (1)$$

where W represents the moisture content of each layer of the skin, and X denotes the amount of tissue fluid replaced with OCA. n_T, n_a, and n_w are the scattering component, the photorefractive agent, and the refractive index of water, respectively. k represents the epidermis, dermis, and blood vessels. The refractive index of scattering particles in skin tissue is assumed to be 1.5. The refractive indexes of glycerol, PEG 400, and glucose are 1.47, 1.468, and 1.39, respectively.

Assuming that size, volume fraction, refractive index of scatters, and thickness of skin tissue remain constant after adding OCA, Mie scattering theory can be used to calculate the scattering coefficient of skin tissues after OCA addition[15]:

$$\mu_s = \mu'_s/(1 - g), \quad (2)$$

$$\mu'_s(\lambda) = \frac{3}{4}\frac{\phi}{\pi a^3}\sigma'_s, \quad (3)$$

where a and ϕ are the radius and volume fraction of scatterers for each layer, respectively. The reduced scattering cross-section σ'_s can be calculated as follows:

$$\sigma'_s = \sigma_s(1 - g)$$

$$= 3.28\pi a^2\left(\frac{2\pi a}{\lambda}\right)^{0.37}(n_s/n_i - 1)^{2.09}, \quad (4)$$

where n_s and n_i are refractive indexes of scatter and background matrix, respectively.

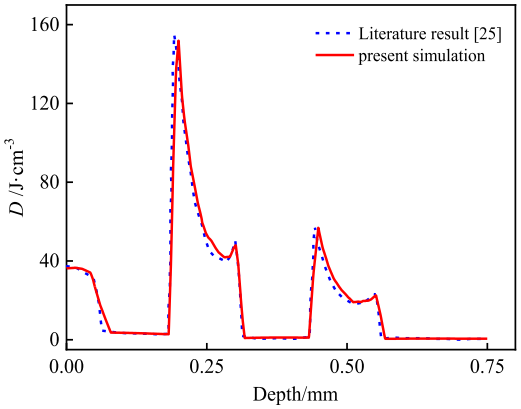

Fig. 2. Comparison of energy deposition along the skin depth.

2.4. *Model validation*

According to Guo *et al.*'s work,[25] the skin model was irradiated by a 595 nm laser with incident energy density of 1 J/cm^2 and spot diameter of 1 mm. The calculated energy deposition along the center axis in the depth direction of the skin was obtained.

The energy deposition along the center axis of the depth direction was compared with the literature result[29] to verify the accuracy of the Monte Carlo method; two discrete blood vessels with a diameter of 120 μm and depths of 250 and 500 μm were considered. According to Guo *et al.*'s work,[25] the skin model was irradiated by a 595 nm laser with incident energy density of 1 J/cm^2 and spot diameter of 1 mm. The calculated energy deposition along the center axis in the depth direction of the skin was obtained. Figure 2 shows that the numerical simulation result agrees well with that of Guo *et al.*,[25] which verifies the accuracy of the Monte Carlo method.

3. Results and Discussion

3.1. *Effect of OCA on light propagation in 808 nm*

The effect of OCA type on the photon transmission in skin tissues was investigated in this section with laser wavelength of 808 nm, spot diameter of 1.0 mm, and incident energy of 1 J/cm^2. Figure 3 shows photon deposition in skin tissues after replacing different proportions of water with PEG 400 based on the assumption that the proportion of tissue fluids replaced with OCAs is 10%–90%. The scattering coefficient in the tissue decreases with the increase in the replaced amount of water with OCA.

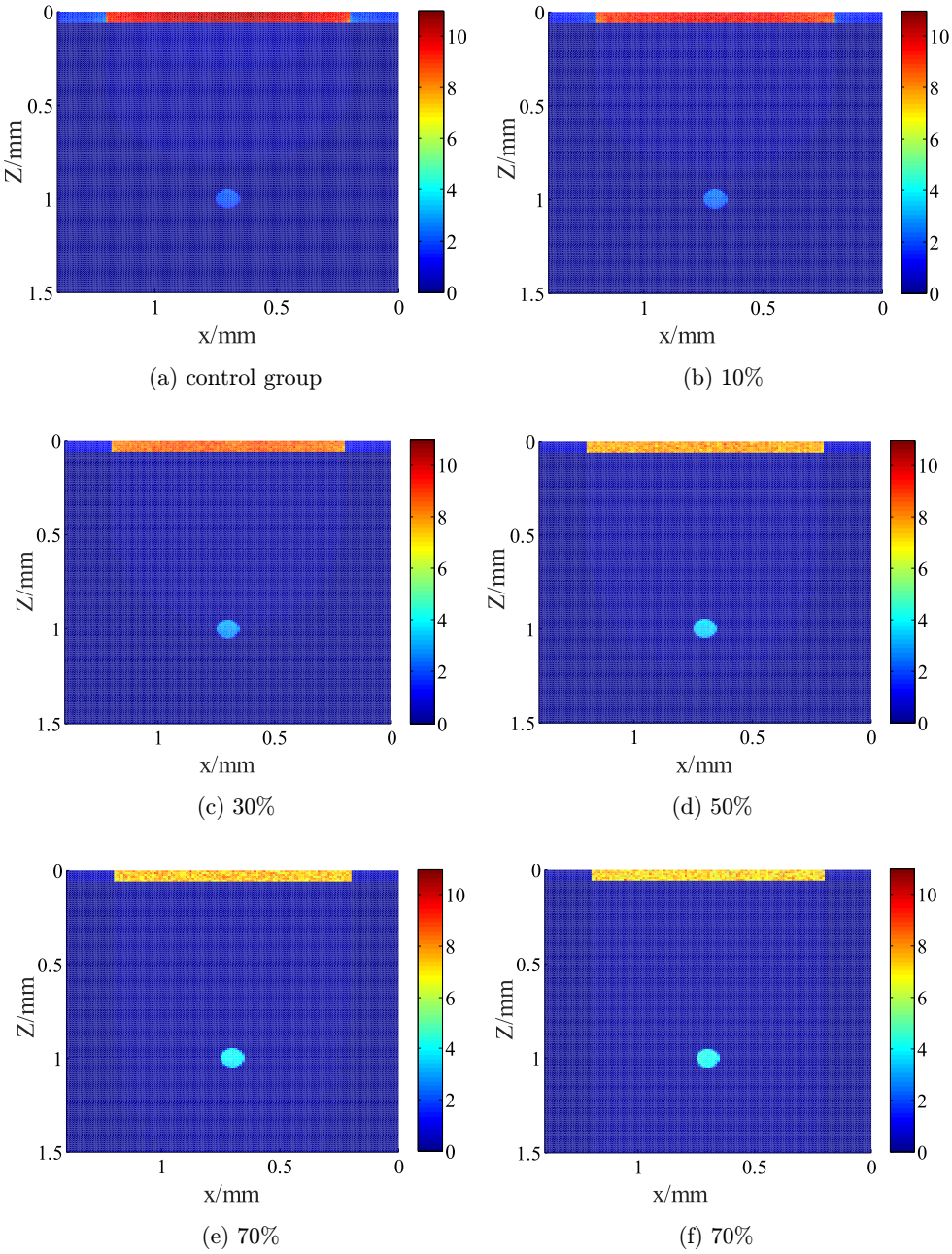

(a) control group (b) 10%

(c) 30% (d) 50%

(e) 70% (f) 70%

Fig. 3. Effect of OCAs on two dimensional photon deposition (OCA: PEG 400).

The photon deposition in the epidermis gradually decreases whereas that in the blood vessel evidently increases.

The axial photon energy deposition E along the incident laser is shown in Fig. 4. Compared with the control group, the photon energy deposition gradually decreases in the epidermis but increases in the blood vessel, and the penetrating depth L in the tissue increases with the replaced content of water with OCA. When X increases from 10% to 90%, the photon energy deposition in the epidermis E_e decreases by 5.96%, 17.02%, 21.85%, 25.05%, and 27.54%, whereas that in the blood vessel E_b increases by 12.31%, 40.93%, 69.79%, 85.88%, and 98.11%. High OCA content leads to considerable photon deposition in blood vessels and deep tissue sampling can be achieved.

Figure 5 shows the effect of three different OCAs on the axial photon deposition when 50% of the tissue fluid is replaced. PEG 400 and glycerol can better increase the photon energy deposition in the target vessel than glucose solution due to their high

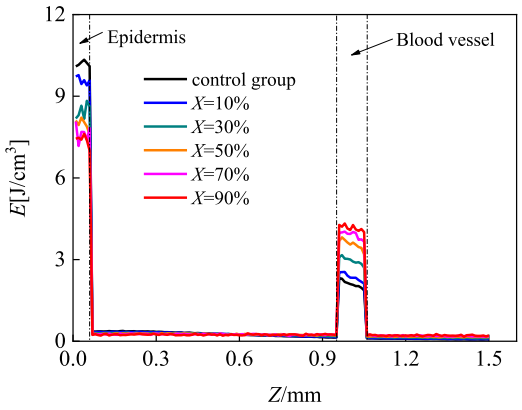

Fig. 4. Effect of PEG 400 on axial photon deposition.

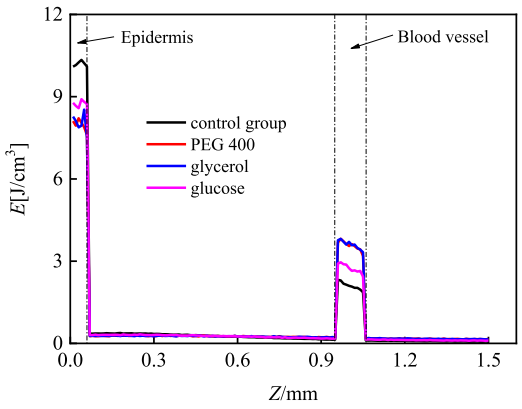

Fig. 5. Effect of different OCAs on axial photon deposition.

refractive index. The increased degrees in the blood vessel are 69.79%, 71.49%, and 30.44% by PEG 400, glycerol, and glucose, respectively.

The average depth of photons transport in skin tissues was simulated with the increase in tissue fluid amount replaced with OCA, as shown in Fig. 6. The photon transport depth in skin tissue increases with the OCA, and the effects of PEG 400 and glycerol on the penetration depth are better than those of glucose. That is, when 50% of tissue fluid is replaced with glycerol, PEG 400, and glucose, the average penetration depth of photons increases by 51.78% (from 0.534 mm to 0.810 mm), 51.06% (from 0.534 mm to 0.806 mm), and 21.51% (from 0.534 mm to 0.648 mm), respectively. Therefore, PEG 400 and glycerol can considerably increase the average penetration depth of photons in skin tissues, thereby raising the sampling depth in LSI for deep blood vessels.

The probability distribution (f) for the photon deposition along the tissue depth was also analyzed,

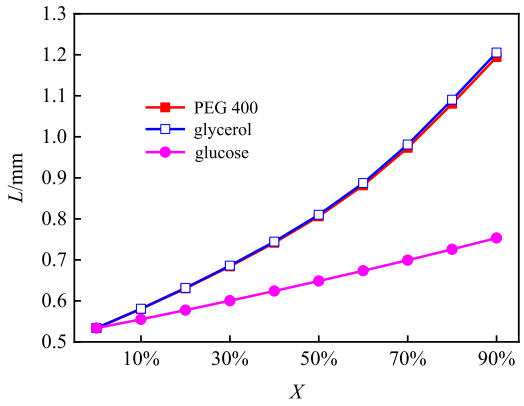

Fig. 6. Effect of water content replacement on penetration depth.

and the results are shown in Fig. 7. With the increase in tissue fluid amount replaced with PEG 400, additional photons move to deep tissues (> 0.65 mm, dash dot line in the figure), showing the gradual decrease in f when tissue depth smaller than 0.65 mm and increase when tissue depth larger than 0.65 mm. Deep tissue information can be detected which increases the sampling depth of the laser speckle system. The maximum probability distribution increases from 0.25 mm depth ($X = 0$) to the depth 1.05 mm ($X = 90\%$), which is the location of deeply buried blood vessels.

The optical clearing effect of PEG 400 (50% replacement of tissue fluid) on blood vessels with different diameters and buried depths was investigated. The optical clearing effect on different vessel diameters (50, 100, and 300 μm) was first studied when the vessel depth is 1 mm. After the action of PEG 400, E_e decreases by 23.51%, 21.85%, and

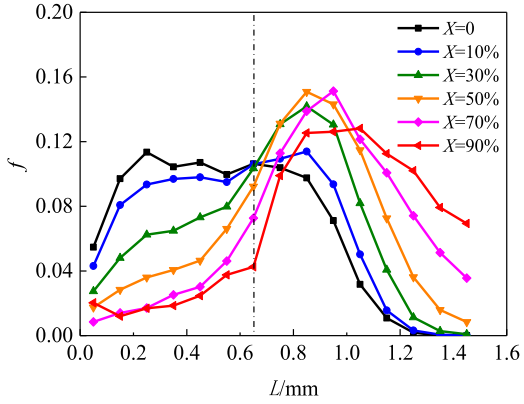

Fig. 7. Probability distribution of average propagation depth with additional PEG 400.

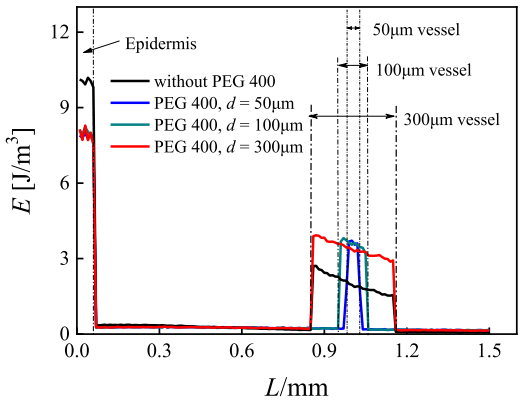

Fig. 8. Effect of PEG 400 on axial photon deposition with different blood vessels diameter.

21.23%, whereas E_b increases by 70.75%, 69.79%, and 68.19%, respectively (Fig. 8).

The photon energy deposition in blood vessels at different buried depths L (0.25, 0.50, 0.75, 1.00, and 1.25 mm) was then studied with vessel diameter of 100 μm. As shown in Fig. 9, PEG 400 can substantially increase E_b by 27.56%, 69.79%, and 112.24% when L is larger than 0.75, 1.00, and 1.25 mm, respectively. E_b decreases after the addition of OCA for the shallow blood vessels. When the vessel depth is 0.25 mm, the photon deposition decreases by 22.74%. Energy deposition in blood vessels mainly comes from photon deposition along depth direction and photon scattering from surrounding tissues, and the former is dominant. The scattering coefficient of tissues decreases with the addition of OCA for shallow blood vessels, and the number of scattered photos from surrounding tissues in blood vessels decreases. The amount of photons scattered from surrounding tissues decreases after the addition of OCA for deep blood vessels, but photon considerably propagates along with the axial depth. Therefore, the effect of OCA on deep blood vessels and sampling depth is crucial.

3.2. *Effect of OCA on light propagation in* 632.8 *nm*

The probability distribution of the average depth of photon propagation in the tissue is shown in Fig. 10. As the degree of light clearness increases, the maximum probability depth of photon penetration in the tissue gradually increases from 0.15 mm to approximately 0.85 mm, which is close to the buried depth of the blood vessel. That is, as the scattering of skin tissue decreases, the number of photons reaching the deep layers of the tissue increases, and the probability of distribution in deep tissues increases. The maximum probabilistic penetration depth of photons at 632.8 nm is slightly less than that at 808 nm mainly because photons are absorbed less by tissues in the near-infrared band, and photons can reach deep skin tissues.

The effect of PEG 400 ($X = 50\%$) on the energy deposition under 808 nm laser in blood vessels of different diameters is shown in Fig. 11. The addition of OCA can effectively reduce the photon energy deposition density in the epidermis, and the diameter of the blood vessel has minimal effect on the photon energy deposition in the epidermis. For a blood vessel with diameters of 50, 100, or 300 μm, E_b increases from 5.57 J·cm^{-3} to 10.56 J·cm^{-3}, 6.30 J·cm^{-3} to 11.95 J·cm^{-3}, and 4.77 J·cm^{-3} to 9.71 J·cm−3 (89.46%, 89.74%, and 103.74%), respectively. For blood vessels of different diameters, PEG 400 can substantially increase the photon

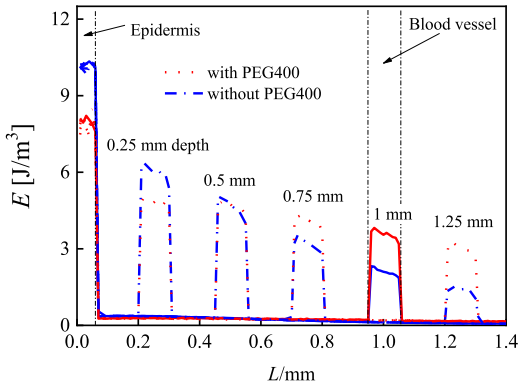

Fig. 9. Effect of PEG 400 on axial photon deposition with different vessel burying depth 606.

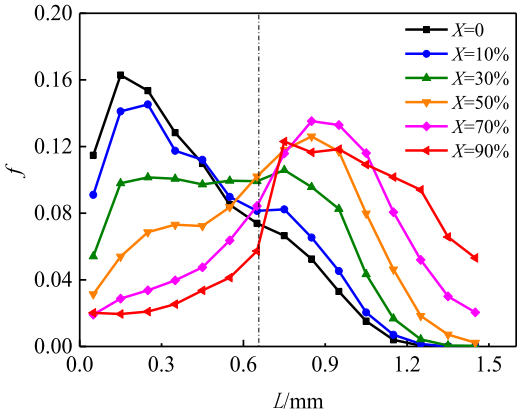

Fig. 10. Probability distribution of average propagation depth with additional PEG 400.

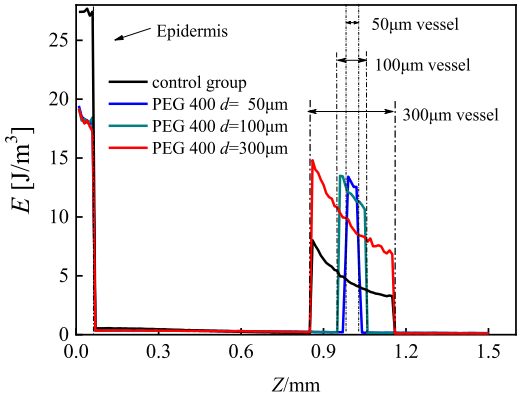

Fig. 11. Effect of PEG 400 on axial photon deposition with different blood vessels diameter.

energy deposition density in the blood vessel, the penetration depth of photons in the tissue, and the sampling depth of the laser speckle. Compared with 808 nm laser, the optical cleaning effect of 632.8 nm laser is evident.

Figure 12 shows the effect of OCA on photon energy deposition under 632.8 nm laser with different burial depths. The diameter of the blood vessel is 100 μm, and the burial depths are 0.25, 0.5, 0.75, 1.0, and 1.25 mm. The incident energy of the laser is 1 J·cm^{-2}. As shown in the figure, when the burial depth of the blood vessel is 0.25 mm, E_b decreases from 28.71 J·cm^{-3} to 21.62 J·cm^{-3} with PEG 400, which is lower than that in the control group. When the burial depths of the blood vessel are 0.5, 0.75, 1.0, and 1.25 mm, E_b increases from 18.53 J·cm^{-3} to 19.41 J·cm^{-3}, from 10.77 J·cm^{-3} to 15.68 J·cm^{-3}, from 63.00 J·cm^{-3} to 119.54 J·cm^{-3}, and from 38.27 J·cm^{-3} to 93.58 J·cm^{-3} (4.72%, 45.60%, 89.74%, and 144.55%), respectively, compared with the control group. For blood vessels with a depth of less than 0.5 mm, the OCA reduced the photon energy deposition in the blood vessels, and the photon energy deposition effect on the blood vessels is evidently increased for the deeply buried blood vessels. Compared with the 808 nm laser, the 632.8 nm laser exhibits increased photon deposition in the skin tissue mainly because the absorption of skin tissue in visible bands is higher than that in near-infrared bands.

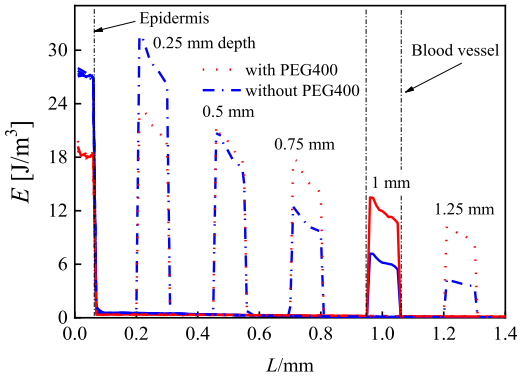

Fig. 12. Effect of PEG 400 on axial photon deposition with different vessel burying depth.

3.3. *Selection of OCA*

The preceding simulation implies that PEG 400 and glycerol can significantly improve the sampling depth of LSI. An *in vivo* experiment was designed in this section to evaluate the optical clearing effect of PEG 400 and glycerol by using SD female mice weighing from 120 g to 150 g, as shown in Fig. 13. After the mice were completely anesthetized, their back hair was shaved, and a twofold skin at the back was lifted. One side was removed with 1 cm diameter circle and fixed by titanium alloy which allowed direct observation of capillaries of the subdermal skin. This observation window was placed in front of the lens of a microscope (SMZ 745T, Nikon, Japan).

Combined with in-house contrast analysis software, a reflective LSI system was established. A continuous He–Ne laser with a wavelength of 632.8 nm (HNL100LB, THORLABS, USA) was used as the light source. The laser has high power stability, low noise level, and excellent inherent beam quality, making it superior to diode lasers. With the power of 10 mW, the laser will not damage human tissues. The LSI of blood vessels was recorded with a CCD camera (Infinity 3-1M, Lumenera, Canada) with a resolution of 1392 × 1040 pixels.

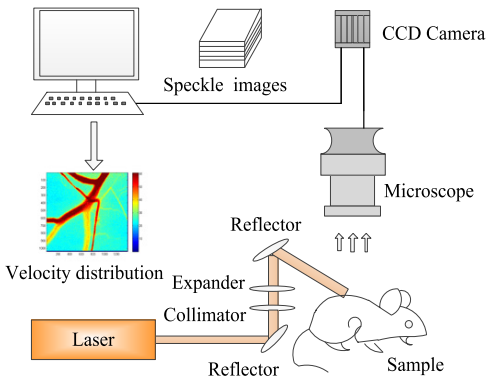

Fig. 13. Schematic of LSI experimental system.

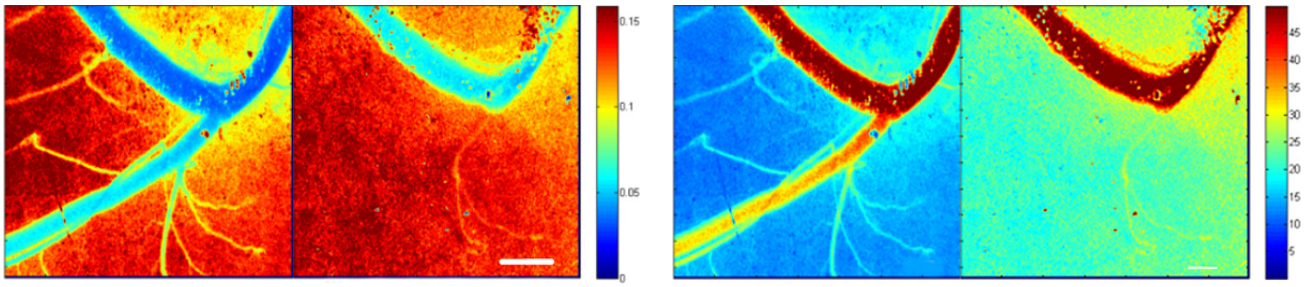

(a) Speckle contrast image (b) Relative velocity distribution

Fig. 14. Speckle contrast image (a) and relative velocity distribution (b) of dorsal blood vessel without (left) and with (right) glycerol clearing. Scale bar 200 μm.

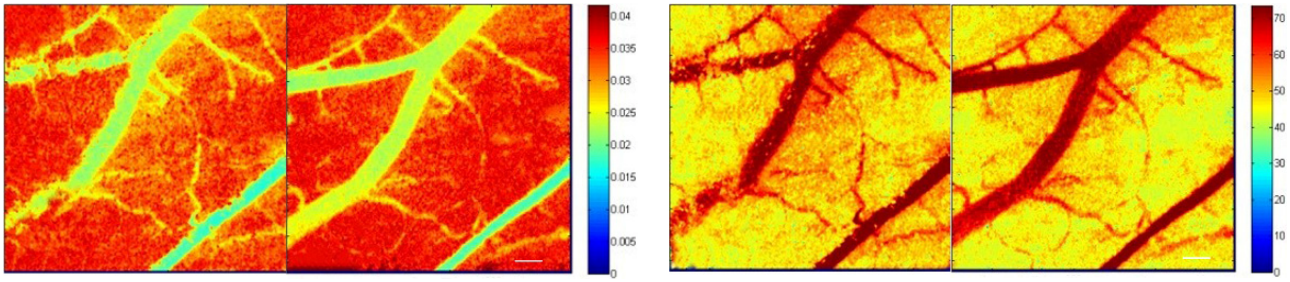

(a) Speckle contrast image (b) Relative velocity distribution

Fig. 15. Speckle contrast image (a) and relative velocity distribution (b) of dorsal blood vessel without (left) and with (right) PEG 400 clearing. Scale bar 200 μm.

Speckle patterns of blood vessels without and with 1 ml of glycerol for 10 min are shown in Fig. 14, respectively. Speckle contrast and relative velocity distribution were calculated by statistical analysis. The figure shows that the addition of glycerol will cause the disappearance of micrangium, and a substantial decrease (by 65%) in blood flow velocity or even stagnation of blood flow is observed. The relative velocity in blood vessels is almost slightly different from that in the surrounding tissue for the considerable decrease in velocity. This condition is mainly due to the imbalance of the equilibrium environment in the blood vessels caused by the addition of glycerol, the aggregation of red blood cells, and the decrease in blood flow velocity or the stagnation of blood flow. Although glycerol shows good optical clearing effect in the simulation, it is unfavorable for the monitoring of blood flow in clinical application.

Figures 15 show the effect of PEG 400 on speckle imaging. After adding 1 ml of PEG 400 for 10 min, the imaging effect is remarkably improved, that is, blood vessels are clear, and the influence on the blood flow is small. With the same increasing sampling depth, PEG 400 shows better imaging effect than that of glycerol by matching refractive indexes in tissues.

Collagen is the main scatterer in the skin, and the hydrogen bonding in collagen triple helix is the main linkage force. OCAs containing hydroxyl group have strong electronegativity which can disturb the high order structure of collagen and cause dissociation. Thus, water molecules in collagen can be replaced with OCAs, and the degree of the internal refractive index matching of the tissue is improved and the sampling depth is increased. Glycerol has more hydroxyl groups than those of PEG 400, and the combination of glycerol with surrounding tissues is stronger than that with PEG 400. The change in the environment in the blood vessels is considerable with glycerol, thus resulting in the polymerization of red blood cells and the reduction or even stagnation of blood flow. PEG 400 can considerably improve the light penetration capability in biological tissues and avoid a significant decrease in blood flow velocity.

4. Conclusion

A double-layer skin tissue model with a single blood vessel was established in this study. The Monte Carlo method which provides theoretical guidance for improving the sampling depth of speckle imaging was used to simulate the photon transport process under the action of light-permeating agents this simulation. An 808 nm semiconductor laser in near-infrared and 632.8 nm He–Ne laser in visible light were selected to study the effect of OCAs on the photon deposition in tissues.

This study shows that the photon energy deposition density in the epidermis increases with the amount of tissue fluid replaced with OCAs. Compared with glucose solution, PEG 400 and glycerol can substantially increase the average penetration depth of photons in the skin tissue and the sampling depth of the LSI. After the action of glycerol, PEG 400, and glucose, the average penetration depth of the photon for the 808 nm laser is increased by 51.78%, 51.06%, and 21.51%, respectively. The sampling depth of speckle imaging by the 632.8 nm laser is lower than that by 808 nm laser. The average penetration depth of the photon is increased by 68.93%, 67.94% and 26.67% after the actions of glycerol, PEG 400 and glucose, respectively.

In vivo experiments were conducted by using a dorsal skin chamber model. PEG 400 can help match the refractive index in tissues and remarkably improves the light penetration in biological tissues. Without causing a large effect on the velocity of blood vessels, PEG 400 exhibits a considerable potential in the monitoring of blood flow. The addition of glycerol can cause a substantial decrease in blood flow rate or even stagnation, which is unconducive to the blood flow monitoring. In laser therapies, such as PWS treatment, blood flow reduction or stagnation will accelerate the thermal damage of the blood vessels and improve the therapeutic effect.

Acknowledgment

This study is financially supported by the National Natural Science Foundation of China (Grant No. 51727811).

References

1. G. Aguila, B. Choi, M. Broekgaarden, O. Yang, B. Yang, P. Ghasri, J. K. Chen, R. Bezemer, J. S. Nelson, A. M. Drooge, A. Wolkerstorfer, K. M. Kelly, M. Heger, "An overview of three promising mechanical, optical, and biochemical engineering approaches to improve selective photothermolysis of refractory port wine stains," *Ann. Biomed. Eng.* **40**, 486–506 (2012).
2. J. C. Alper, L. B. Holmes, "The incidence and significance of birthmarks in a cohort of 4641 newborns," *Pediatr. Dermatol.* **1**, 58–68 (1983).
3. R. Anderson, J. Parrish, "Selective photothermolysis: Precise microsurgery by selective absorption of pulsed radiation," *Science*, **220**, 524–527 (1983).
4. D. Li, R. Li, H. Jia, B. Chen, W. J. Wu, Z. X. Ying, "Experimental and numerical investigation on the transient vascular thermal response to multi-pulse Nd:YAG laser," *Lasers Surg. Med.* **49**, 852–865 (2017).
5. S. Kimel, L. O. Svaasand, M. J. Hammer-Wilson, J. Stuart Nelson, "Influence of wavelength on response to laser photothermolysis of blood vessels: Implications for port wine stain laser therapy," *Lasers Surg. Med.* **33**, 288–295 (2003).
6. J. D. Briers, A. F. Fercher. "Retinal blood-flow visualization by means of laser speckle photography," *Invest. Ophthalmol. Vis. Sci.* **22**, 255–259 (1982).
7. J. D. Briers, S. Webster, "Laser speckle contrast analysis (lasca): A nonscanning, full-field technique for monitoring capillary blood flow," *J. Biomed. Opt.* **1**, 174–179 (1996).
8. M. Draijer, E. Hondebrink, T. Leeuwen, W. Steenbergen, "Review of laser speckle contrast techniques for visualizing tissue perfusion," *Lasers Med. Sci.* **24**, 639–651 (2009).
9. P. Miao, A. Rege, N. Li, N. V. Thakor, S. Tong, "High resolution cerebral blood flow imaging by registered laser speckle contrast analysis," *IEEE Trans. Biomed. Eng.* **57**, 1152–1157 (2010).
10. B. Ruth, "Measuring the steady-state value and the dynamics of the skin blood flow using the non-contact laser speckle method," *Med. Eng. Phys.* **16**, 105 (1994).
11. Q. Liu, Z. Wang, Q. M. Luo, "Temporal clustering analysis of cerebral blood flow activation maps measured by laser speckle contrast imaging," *J. Biomed. Opt.* **10**, 024019 (2005).
12. H. Y. Cheng, Q. M. Luo, S. Q. Zeng, J. Cen, W. N. Liang, "Optical dynamic imaging of the regional blood flow in the rat mesentery under the effect of noradrenalin," *Prog. Nat. Sci. Mater. Int.* **13**, 397–400 (2003).
13. J. O'Doherty, P. Mcnamara, N. T. Clancy, J. G. Enfield, M. J. Leahy, "Comparison of instruments for investigation of microcirculatory blood flow and red blood cell concentration," *J. Biomed. Opt.* **14**, 034025 (2009).

14. A. B. Parthasarathy, W. J. Tom, A. Gopal, X. J. Zhang, A. K. Dunn, "Robust flow measurement with multi-exposure speckle imaging," *Opt. Exp.* **16**, 1975–1989 (2008).
15. A. N. Bashkatov, E. A. Genina, V. T. Valery, B. A. Gregory, V. Y. Yaroslavsky, "Monte Carlo study of skin optical clearing to enhance light penetration in the tissue: implications for photodynamic therapy of acne vulgaris," *Proc. Spie* **19**, 1601–1612 (2007).
16. G. Vargas, E. K. Chan, J. K. Barton, H. G. Rylander, III and A. J. Welch, "Use of an agent to reduce scattering in skin," *Lasers Surg. Med.* **24**, 133–141 (1999).
17. E. I. Galanzha, V. V. Tuchin, A. V. Solovieva, T. V. Stepanova, Q. Luo, H. Cheng, "Skin backreflectance and microvascular system functioning at the action of osmotic agents," *J. Phys. D. Appl. Phys.* **36**, 1739–1746 (2003).
18. W. Feng *et al.*, "Skin optical clearing potential of disaccharides," *J. Biomed. Opt.* **21**, 081207 (2016).
19. H. Y. Cheng, Q. M. Luo, S. Q. Zeng, W. H. Luo, H. Gong, "Hyperosmotic chemical agent's effect on in vivo cerebral blood flow revealed by laser speckle," *Appl. Opt.* **43**, 5772–5777 (2004).
20. W. Jing *et al.*, "Tissue optical clearing window for blood flow monitoring," *IEEE J. Sel. Top. Quantum Electron.* **20**, 92–103 (2013).
21. S. Rui *et al.*, "Accessing to arteriovenous blood flow dynamics response using combined laser speckle contrast imaging and skin optical clearing," *Biomed. Opt. Exp.* **6**, 1977–1989 (2015).
22. H. Yu *et al.*, "Collaborative effects of wavefront shaping and optical clearing agent in optical coherence tomography," *J. Biomed. Opt.* **21**, 121510 (2016).
23. G. Li *et al.*, "Optical coherence tomography angiography offers comprehensive evaluation of skin optical clearing in vivo by quantifying optical properties and blood flow imaging simultaneously," *J. Biomed. Opt.* **21**, 081202 (2016).
24. J. Wang, R. Shi and D. Zhu, "Switchable skin window induced by optical clearing method for dermal blood flow imaging," *J. Biomed. Opt.* **18**, 061209 (2012).
25. M. J. C. van Gemert *et al.*, "Skin optics," *IEEE Trans. Biomed. Eng.* **36**, 1146–1154 (1989).
26. L. H. Wang, S. L. Jacques and L. Q. Zheng, "Mcml-monte carlo modeling of light transport in multi-layered tissues," *Comput. Methods Programs Biomed.* **47**, 131–146 (1995).
27. W. He, Research on improving the sampling depth of laser speckle blood flow imaging. Ph.D Thesis, Huazhong University of Science and Technology (2012).
28. V. V. Tuchin, "Optical clearing of tissues and blood," *J. Phys. D. Appl. Phys.* **38**, 2497–2518 (2005).
29. Z. X. Guo, A. Janice, A. G. Bruce and S. Kumar, "Monte carlo simulation and experiments of pulsed radiative transfer," *J. Quant. Spectrosc. Radiat. Transf.* **73**, 159–168 (2002).